A COMPARISON BETWEEN EXPERIMENTAL AND NUMERICAL ANALYSIS OF A WELLS TURBINE

T Ghisu - P. Puddu - F. Cambuli

Department of Mechanical, Chemical and Materials Engineering
University of Cagliari, via Marengo 2, Cagliari (Italy)
Email t.ghisu@unica.it

ABSTRACT
Wave energy is one of the renewable energy sources with the highest potential. Several pilot plants have been built based on the principle of the Oscillating Water Column (OWC). Among the different solutions that have been suggested, the Wells turbine has gained particular attention due to its simplicity and reliability.
The majority of available studies concentrate on the steady operation of the Wells turbine, while only few analyze its performance under an unsteady and bi-directional air flow, as determined by the presence of the OWC system.
In this work, experimental and numerical performance of a high-solidity Wells turbine with NACA0015 profiles under the bi-directional flow generated by a hydraulic piston is compared. The numerical simulations have been conducted using commercial CFD software and focus on unsteady predictions, with particular attention to the behavior of the flow upstream and downstream of the rotor, flow hysteresis between acceleration and deceleration phases and differences between intake and exhaust strokes due to the non-symmetrical configuration of the machine.

NOMENCLATURE
F_t tangential force per unit length
F_t tangential force per unit length
P static pressure
P^* non-dimensional static pressure drop
P^{**} non-dimensional static pressure drop (with local flow variables)
$\underline{f}$ piston frequency
$\overline{f}$ non-dimensional piston frequency
c blade chord
r radius
$r*$ non-dimensional radius $(r - r_h)/(r_t - r_h)$
r_t tip radius
r_h hub radius
T torque
T^* non-dimensional torque
T^{**} non-dimensional torque (with local flow variables)
U blade speed
V_a axial velocity (absolute)
V_t tangential velocity (absolute)
W_a axial velocity (relative)
W_t tangential velocity (relative)
ϕ flow coefficient
ϕ_l local flow coefficient
ω rotational speed
ρ density

INTRODUCTION

Among the various sources of renewable energy, sea wave power has the highest energy potential and it is easily predictable. Its high intensity makes the resource of wave energy very attractive for contributing to satisfy the demand for electricity worldwide. To convert this energy potential into electrical energy it is important to employ particularly efficient wave motion conversion devices (Thorpe (2000); Taylor (1983); de O. Falcao (2010)).

The most interesting devices designed for the extraction of wave energy are the ones based on the principle of the oscillating water column (OWC). Such systems are composed of two units: the system that captures and converts the energy of wave motion into pneumatic energy at low pressure to produce a bi-directional airflow and the turbo-generator driven by this flow. This configuration presents the advantage of ensuring simplicity of construction and safety of operation.

The unsteady and bi-directional flow generated by wave motion requires the use of specific turbines that can operate under these conditions. Of particular interest are the one proposed by A. Wells (Wells (1976); Raghunathan (1995); Gato and de O. Falcao (1988)) and the impulse turbine (Setoguchi et al. (2001)). The analysis of the flow through these turbines has been carried out with experimental, analytical and numerical methods. Setoguchi and Takao (2006) present a detailed review and comparison of the performance of several types of self-rectifying air turbines for energy conversion, including Wells turbines with and without guide vanes, turbines with self-pitch-controlled blades, biplane Wells turbine with guide vanes and contra-rotating Wells turbines. Curran and Gato (1997) experimentally investigated the performance of several designs, while Thakker and Abdulhadi (2007) studied the effect of airfoil shape and blade solidity on the performance of a monoplane Wells turbine, both under simulated (sinusoidal) and real flow conditions. A number of authors have proposed methods for increasing the low efficiency of Wells turbines: Kim et al. (2002b) and Setoguchi et al. (2003) studied the use of variable pitch blades, Govardhan and Dhanasekaran (1998) introduced guide vanes to direct the incoming flow in the direction of rotation with the effect of increased torque and efficiency, but at the price of a narrower operating range; Gato and Webster (2001) proved the positive effect of backward sweep on the operating range of both pitched and unpitched symmetrical (NACA0015) blades (at the price of a reduction in peak efficiency).

In recent years, thanks to the increase in computational power and the development of more efficient numerical approaches, a number of studies have used Computational Fluid Dynamics (CFD) to predict the performance of Wells turbines. In consideration of the low frequencies of sea waves, most authors have used a steady approach: Kim et al. (2001) investigated the effect of blade hub-to-tip and aspect ratios on turbine torque and efficiency, Kim et al. (2002a) used the same method to predict the optimal value of blade sweep for both NACA0020 and CA9 blades, reaching the same comclusion otained by Govardhan and Dhanasekaran (1998) in their experimental work. Kinoue et al. (2003) used an unsteady approach to predict the hysteresis between acceleration and deceleration strokes found in the Wells turbine studied by Setoguchi et al. (1998). Dhanasekaran and Govardhan (2005) employed an unstructured grid to predict the performance of a NACA0021 Wells turbine under attached and separated flow conditions, with reasonable accuracy.

Although some of these studies have highlighted specific issues linked to unsteady flow characteristics, most of them have been carried out with uniform and stationary flow conditions, mainly because of the complexities related to flow generation and measurement of fluid dynamic and mechanical quantities under turbine unsteady operation (experimental studies) and large computational requirements for simulating the complete wave generation system or early stall operating conditions (numerical works). The reasons for the presence of a hysteretic cycle, highlighted in a number of studies (Setoguchi et al. (1998); Kinoue et al. (2003), has been attributed by the same authors to the different aerodynamic performance of the blade during acceleration and deceleration phases. This can be confirmed only if aerodynamic forces are correlated to local kinematic parameters, rather than to the piston position. Furthermore, a clearer understanding of stall and of its dependence on the turbine

geometry is necessary to improve the performance and efficiency of the machine.

An experimental device has been designed and built to simulate OWC systems in the Department of Mechanical, Chemical and Materials Engineering (DIMCM) at the University of Cagliari. Puddu et al. (2014) presented the experimental results for a high-solidity low aspect-ratio Wells turbine equipped with NACA0015 profile blades submitted to an unsteady and bi-directional flow, recontructing in detail the istantaneous flow upstream and downstream of the rotor. In this work, the authors compare these results with the numerical predictions obtained with a commercial CFD software (ANSYS Fluent), with particular attention to flow behavior, hysteresis between acceleration and deceleration phases and differences between intake and exhaust strokes due to the non-symmetrical configuration of the machine.

EXPERIMENTAL SET-UP AND INSTRUMENTATION

The experimental apparatus in use consists of a cylindrical chamber (1m diameter) with a piston moved by a hydraulic actuator reproducing the desired wave motion. A periodic bi-directional flow is achieved through a 0.25 m diameter Wells turbine as in a real OWC plant. The turbine shaft is connected to an asynchronous generator equipped with inverter and feedback encoder that allows to control the rotational speed. The maximum power generated by the turbine is in the order of 240 W. Geometrical parameters are summarized in Table 1. Figure 1 reports a global schematic of the machine, a more detailed view of the turbine, and a skecth of the velocity triangles during outflow and inflow phases. Experimental set-up and detailed analysis of the investigations is reported in Puddu et al. (2014). A single non-dimensional piston frequency has been analyzed ($\overline{f} = f/(\omega r_t c) = 0.065$).

Table 1: Wells turbine data

Airfoil	NACA 0015	Blade Number	14
Rotor Tip Diameter	250 mm	Solidity at Tip Radius	0.642
Rotor Hub Diameter	190 mm	Sweep Ratio	0.417 (15/36)
Chord Length	36 mm	Rotational Speed	3600 rpm
Tip Clearance	1 mm	Piston Period	9 s

While performance of Wells turbine depend on the combined effect of lift and drag, they are uually represented in terms of non-dimensional static pressure difference P^* and torque T^* as a function of flow coefficient ϕ

$$T^* = \frac{T}{\rho\omega^2 r_t^5} \qquad P^* = \frac{\Delta P}{\rho\omega^2 r_t^2} \qquad \phi = \frac{V_a}{\omega r_t} \qquad (1)$$

where ΔP is the pressure difference across the rotor, ρ is the flow density, ω the machine's rotational speed, r_t the tip radius, T the torque and V_a the axial velocity upstream of the rotor.

The set-up was equipped with different sensors to measure the unsteady values of the turbine angular speed, torque, piston position and wall static pressure near the rotor. Besides the global parameters of the turbine, also the flow field near the rotor was studied. A split-fiber film anemometer was positioned alternatively upstream and downstream of the turbine, at the mean turbine radius, to measure the 2D characteristic of the flow. The anemometer was differently oriented during air inflow and outflow phases with a motorized positioning system. Data acquisition was performed for at least one piston stroke, using a high speed multichannel DAQ-board. The data were processed using phase locked ensemble averaging technique.
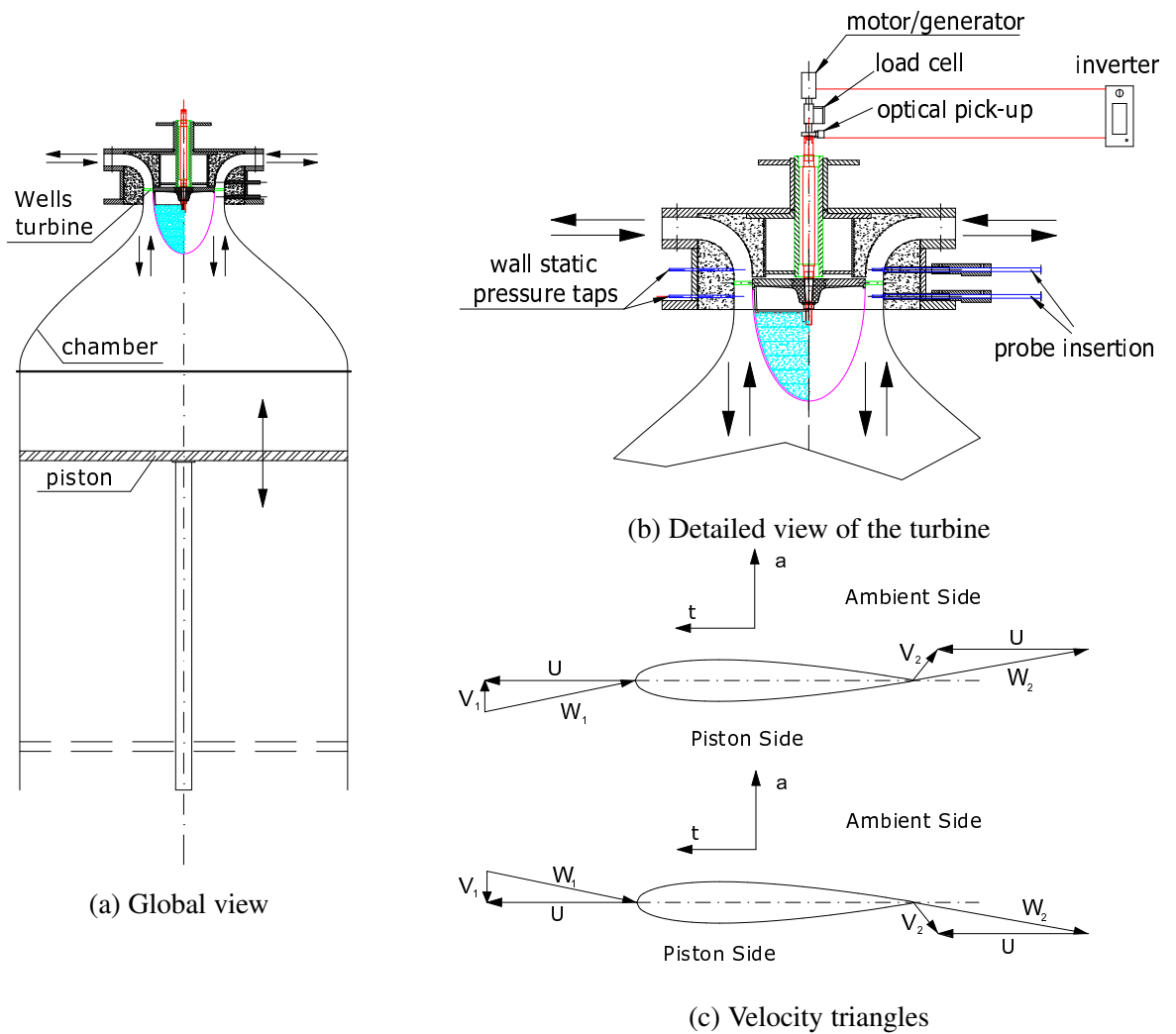
(a) Global view

(b) Detailed view of the turbine

(c) Velocity triangles

Figure 1: **Scheme of the Wells turbine under investigation**

NUMERICAL ANALYSIS

The numerical simulations have been conducted with the commercial CFD software Ansys Fluent 14.0, while Ansys IcemCFD has been used to generate the numerical grid used to approximate the governing equation. The unsteady Reynolds-Averaged Navier-Stokes (RANS) equations have been solved for a compressible ideal gas. In consideration of the low Reynolds number of the machine (between $0.8 \cdot 10^5$ and $1.5 \cdot 10^5$ based on blade chord depending on operating conditions) the flow is likely to be laminar or transitional (Raghunathan, 1995). In order to be able to simulate laminar separation leading to early stall, the transition SST model has been selected for turbulence closure. The SIMPLEC algorithm has been used for pressure-velocity coupling, a second-order upwind scheme for discretizing convective terms and a second-order centered scheme for pressure and viscous terms. Multiple-reference frames have been used for simulating the interaction between stationary and rotating regions. The motion of the piston has been simulated by mean of a moving wall. A user-defined-function (UDF) defines the position of the piston as a function of time, while a dynamic mesh (cell-layering) allows the domain to adapt to the motion of the piston. Due to the presence of a 90 degree curved exit channel, care needs to be taken to avoid a strong influence of boundary conditions on numerical results: a box has been added on the external side of the turbine radial entrance/exit, with the effect that boundary conditions are now specified further away from the region of interest. One blade passage has been simulated, with periodic boundary conditions. A schematic of the computational domain is shown in Figure 2.
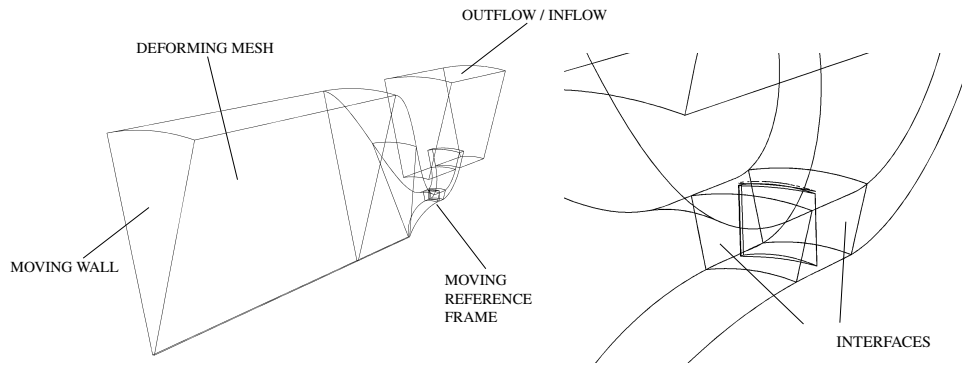
4

Figure 2: **Computational domain**

(a) Blade and hub surface mesh
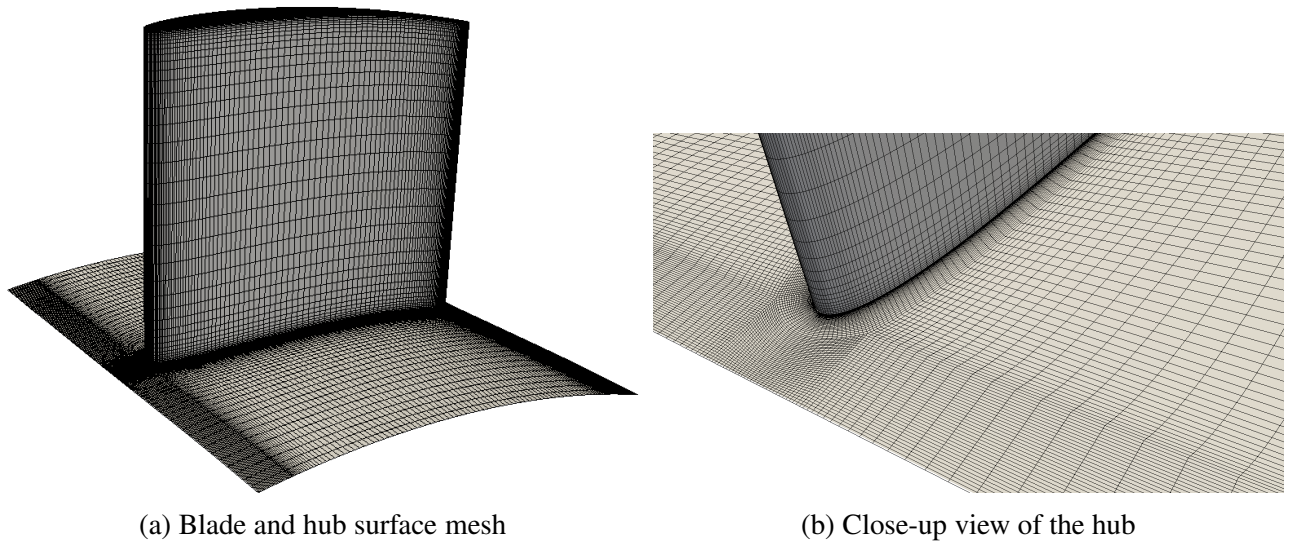
(b) Close-up view of the hub

Figure 3: **Computational mesh for the moving reference frame**

A multi-block structured grid (Figure 3) has been used to discretize the governing equations. A C-grid is used around the blade to capture the complex boundary layer flow (particularly important in the presence of a transitional model), with a H-mesh structure in the rest of domain.

A grid sensitivity study has been conducted to verify the choice of the numerical mesh. For the basic mesh, 260 points have been used around the blade profile, 70 between successive blades (in the wake region). In the spanwise direction, 35 points cover the blade span, while 10 points have been used in the tip gap region, for a total of about one million cells. A finer mesh has been obtained by increasing by 30% the number of grid points in every direction. The maximum y+ is of the order of 1 to ensure a good resolution of the boundary layer. Figure 4 shows the difference in the coefficients of torque and static pressure for coarse and finer mesh (steady-state simulations): while there is a small divergence in the results for higher flow coefficiencts (higher angles of attack) the values obtained with the coarser mesh are acceptable.

RESULTS

Integral analysis

Figure 5 compares the non-dimensional coefficients of torque (Figure 5a) and static pressure drop (Figure 5b) with experimental data. The flow coefficient ϕ is calculated from the piston velocity, assuming the flow at inlet to the turbine to be axial and neglecting compressibility effects. The agreement is satisfactory. The maximum value of torque during the outflow phase (positive ϕ) is
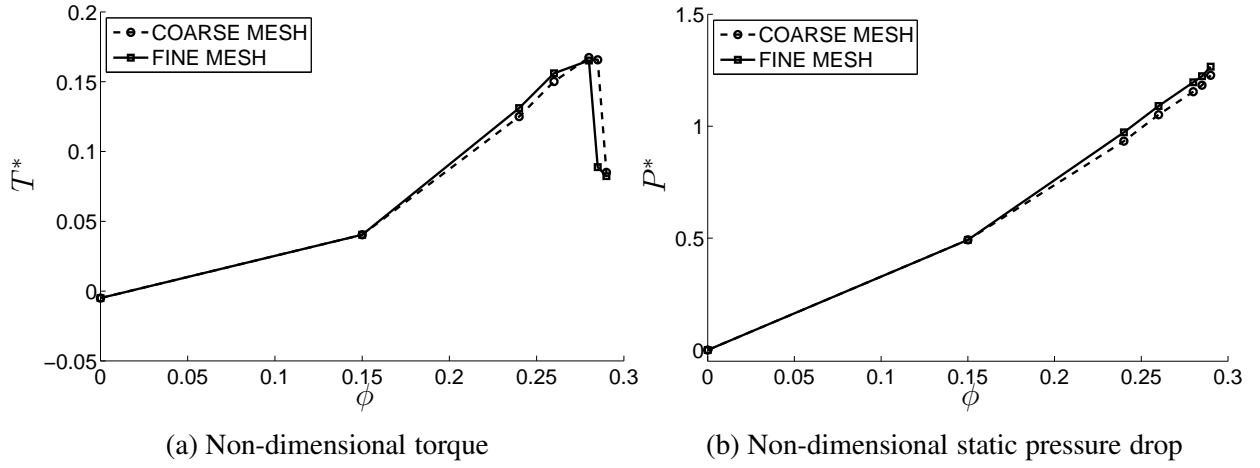
(a) Non-dimensional torque   (b) Non-dimensional static pressure drop

Figure 4: **Mesh verification**

(a) Non-dimensional torque   (b) Non-dimensional static pressure drop
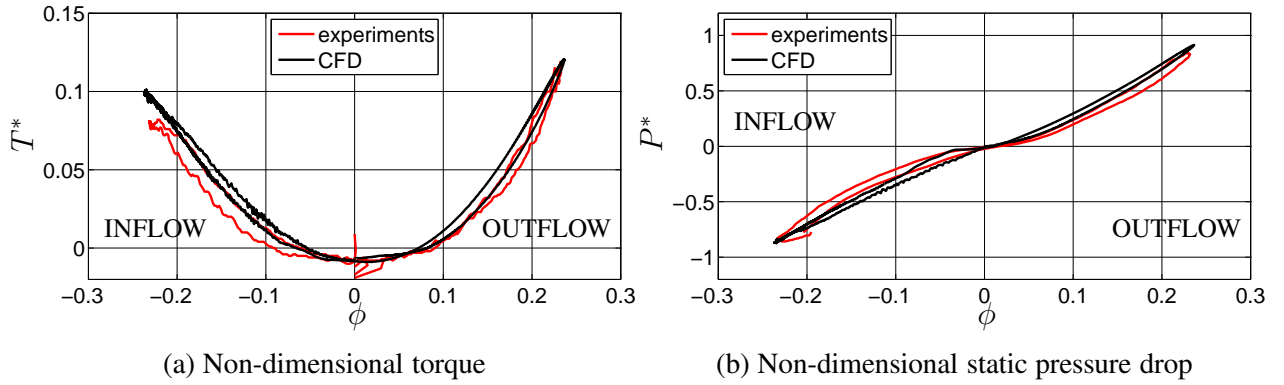
Figure 5: **Comparison between experimental and computational results**

well captured, while the drop in performance recorded in the inflow stroke is slightly underestimated. Positive torque is generated by pressure forces acting on the blade surface, while the contribution given by viscous forces acts in the opposite direction. At low incidence (low values of ϕ) viscous forces prevail, while at the maximum ϕ (0.24) the contribution of viscous forces to torque is about 8% of the torque generated by pressure forces. The presence of a hysteretic behavior (lower values of static pressure drop and torque during acceleration than during deceleration) is also captured.

In order to understand if the hysteresis is generated by different blade aerodynamic performance during acceleration and deceleration (as suggested by Setoguchi et al. (1998); Kinoue et al. (2003)), performance should be correlated to flow characteristics in the proximity of the blade. In the experiments, Puddu et al. (2014) recorded the instantaneous two-dimensional flow at mid-span 20 mm upstream and downstream of the rotor. Figure 6 compares these data with the numerical results (only axial and tangential components of velocity are reported as the flow is predominantly in the blade-to-blade plane). Velocity ratios (velocity components on blade tip speed) are reported as a function of the non-dimensional piston position (where 0 represents the bottom dead center and 1 the top dead center). Figures on the left side represent the inflow phase, while figures on the right side refer to outflow. During the inflow stroke, the flow is axial upstream of the blade and the velocity magnitude is well captured by the numerical analysis (Figure 6a), while the tangential flow component downstream of the blade (Figure 6c) is overestimated, probably because of a flow separation on the suction side
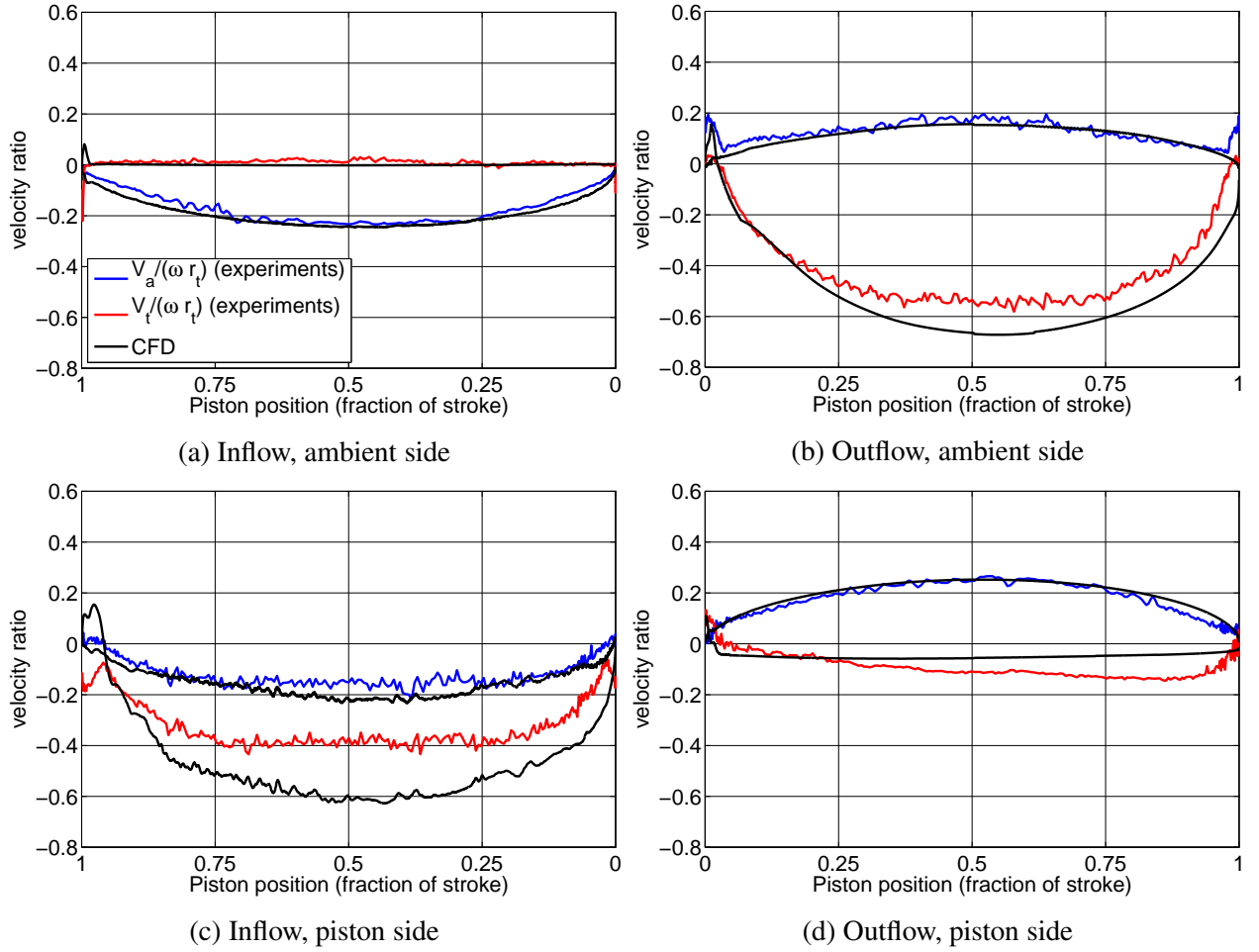
6

Figure 6: **Experimental and numerical velocity components upstream and downstream of the rotor**

of the blade that is not correctly captured (or underestimated) by the numerical analysis, and this is reflected on the overprediction of torque coefficient presented in Figure 5a. During the outflow stroke, while the axial flow component upstream of the blade (Figure 6d) is correctly captured, the tangential component (due to the recirculation of the swirling flow generated during the previous stroke) is underestimated. The difference in flow characteristics upstream of the rotor between inflow and outflow generates different performance during the two phases. Figure 7 reports the measured axial flow velocity (non-dimensionalized with tip speed) upstream of the rotor as a function of the flow coefficient ϕ (calculated based on the piston position). The delay between the two velocities generates a hysteretic loop that is more pronounced during the inflow stroke than during outflow (both in experiments and computations). The modest underestimation of flow velocity can be explained with a non-optimal prediction of boundary layer blockage or radial velocity gradients due to duct curvature.

To verify if the delay reported in Figure 7 is responsible for the hysteretic behavior shown in Figure 5, torque and static pressure drop have been non-dimensionalized with local values of velocity rather than with blade tip speed as in equations 1, and plotted as a function of a local flow coefficient ϕ_l (equations 2). The results, reported in Figure 8, demonstrate how the apparent hysteresis highlighted in Figure 5 is caused by the delay effects introduced by the presence of ducts and chamber and not by specific fluid dynamics responses to flow acceleration and deceleration, as in the works of Setoguchi et al. (1998) and Kinoue et al. (2003).
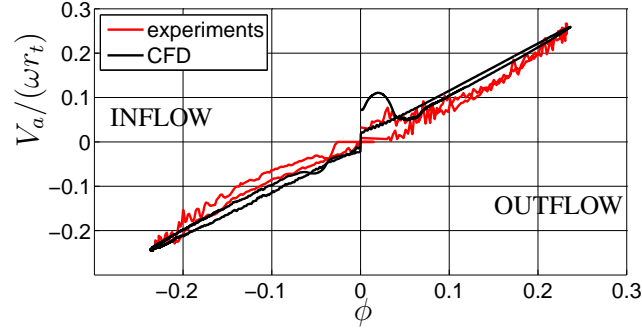
Figure 7: **Relationship between piston velocity and axial flow velocity upstream of the rotor**
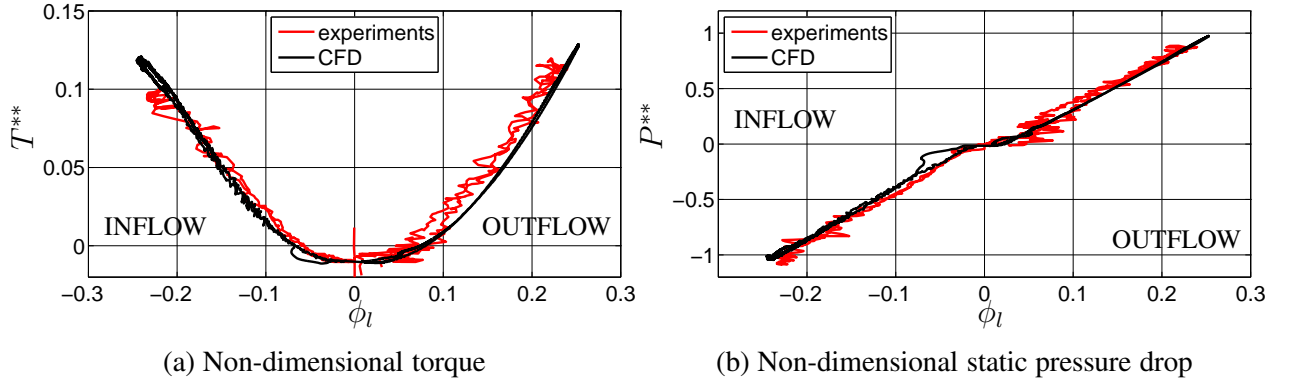

(a) Non-dimensional torque

(b) Non-dimensional static pressure drop

Figure 8: **Computational and experimental performance as a function of local flow variables**

$$T^{**} = \frac{T}{\rho(W_t^2 + W_a^2)r_t^3} \qquad P^{**} = \frac{\Delta P}{\rho(W_t^2 + W_a^2)} \qquad \phi_l = \frac{W_a}{W_t} \tag{2}$$

Radial distributions

The above analysis, while explaining the origin of the hysteresis cycles observed in Figure 5, does not explain the difference in performance between inflow and outflow phases, and the partial leveling off of torque at high negative flow coefficients (during inflow) that can be caused by a partial stall of the blade. To verify this hypothesis, the mass-averaged radial distributions of flow variables at rotor inlet have been analyzed for the CFD analysis. Figure 9 reports radial distributions of axial velocity and local flow coefficient ($\phi_l = W_a/W_t$) for inflow and outflow, at $\phi = 0.15$, evaluated 20 mm upstream of the rotor blade (distributions for other values of ϕ follow similar trends and have not been reported). While the flow is almost uniform during the outflow stroke, the presence of a 90-degree bend generates a strong gradient in the inlet velocity distribution during the inflow stroke (Figure 9a). This is reflected on the values of local flow coefficient (Figure 9b), higher at the tip during inflow despite the larger blade speed (during outflow the hub experiences a higher incidence).

The flow distribution described above increases blade loading at the tip (where also the solidity is lower) and moves the blade closer to a local stall. This can be evinced from the deficit in tangential force in the tip region of the blade shown in Figure 10c, caused by the local angle of attack being larger than the stall angle for the particular working conditions (low Reynolds number). Figure 11 reports the contour plots of relative velocity at 20%, 50% and 80% span, for $\phi = 0.24$: while the flow remains attached during both inflow and outflow at the first two radial position, it starts to separate near the
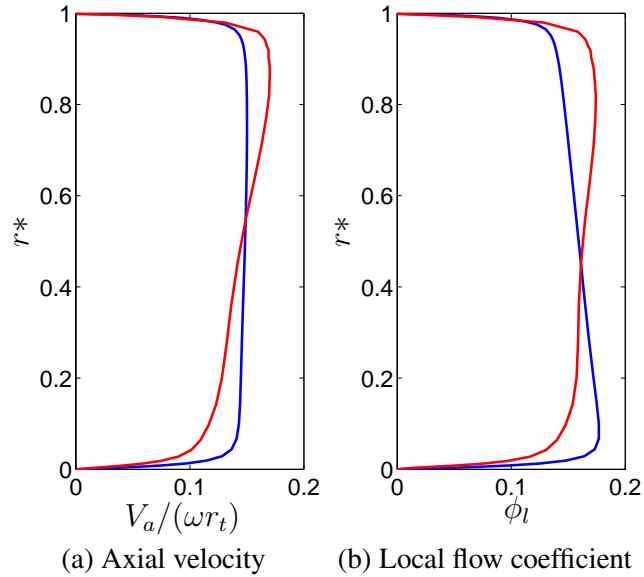
(a) Axial velocity   (b) Local flow coefficient

Figure 9: **Radial flow distributions upstream of the blade (blue outflow, red inflow)**

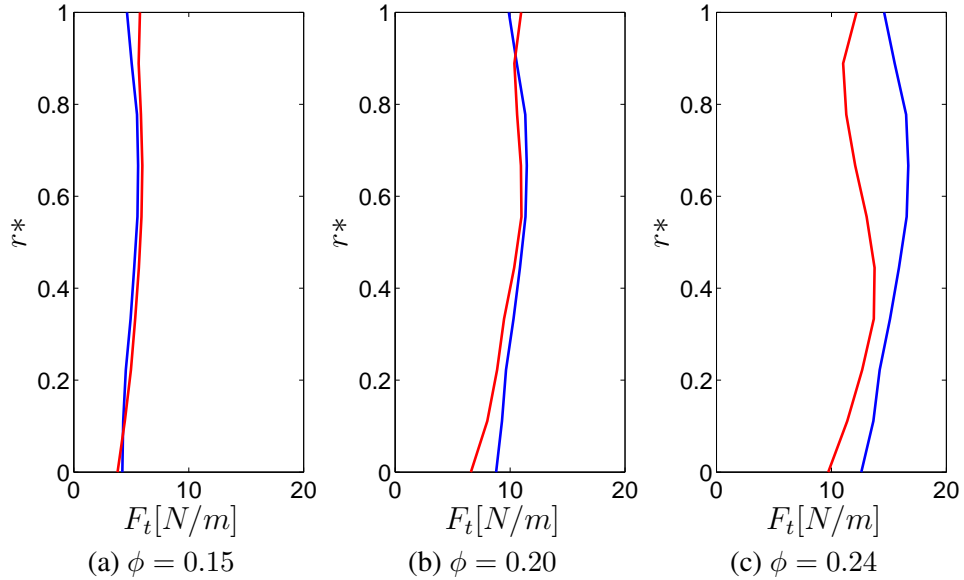(a) $\phi = 0.15$ (b) $\phi = 0.20$ (c) $\phi = 0.24$

Figure 10: **Distributions of tangential force per unit length for different flow coefficients (blue outflow, red inflow)**

blade tip during inflow (Figure 11f) causing the described deficit in torque. This separation (and the consequent lower torque during inflow than during outflow) is not captured by a fully-turbulent turbulence model, as the blade experiences a laminar separation in the presence of a Reynolds number in the order of 10^5.

CONCLUSIONS

This work deals with the numerical analysis of a high-solidity Wells turbine submitted to a periodic bi-directional flow. Numerical results have been compared to the experimental data of Puddu et al. (2014).

The presence of a hysteresis loop has been verified. Setoguchi et al. (1998) and Kinoue et al.

(a) 20% span, outflow   (b) 20% span, inflow

(c) 50% span, outflow   (d) 50% span, inflow

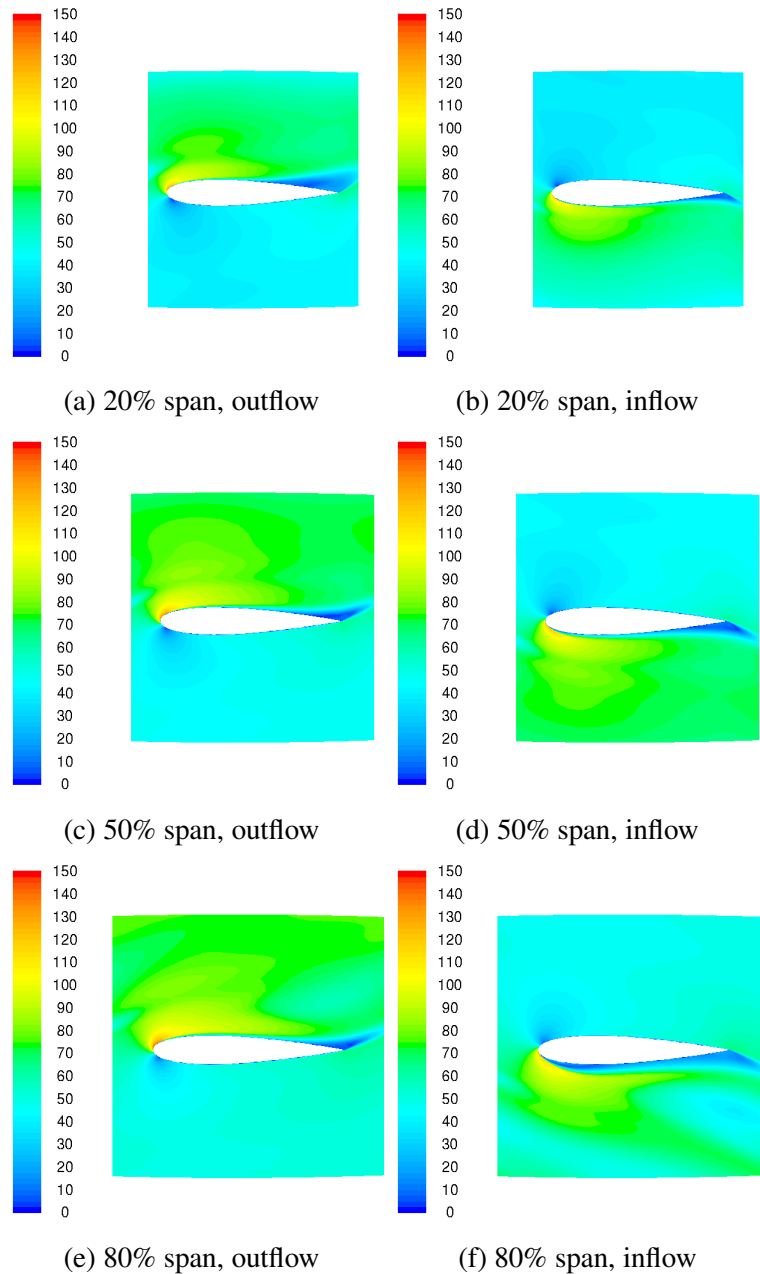(e) 80% span, outflow   (f) 80% span, inflow

Figure 11: **Contour plots of relative velocity (m/s)**

(2003) attributed its presence to the different interaction of the blade wake with the suction side flow during the two phases. In this work, by correlating the performance of the turbine to flow parameters in the proximity of the blade, it has been demonstrated how the different performance can be attributed solely to the delay effects introduced by the presence of ducts and chamber. More analysis is necessary to understand the effects of the turbine geometrical parameters (solidity, aspect ratio, hub-to-tip ratio) on its performance and on the development of hysteresis.

The difference between inflow and outflow strokes have also been analyzed in detail, highlighting how the presence of a curved duct influences the flow distribution during inflow, increasing the tip loading and leading to an early flow separation and deteriorated performance.

10

REFERENCES

Curran, R., Gato, L. M. C., 1997. The energy conversion performance of several types of Wells turbine designs. Proceedings of the Institution of Mechanical Engineers, Part A: Journal of Power and Energy 211 (2), 133–145.

de O. Falcao, A. F., 2010. Wave energy utilization: A review of the technologies. Renewable and Sustainable Energy Reviews 14 (3), 899–918.

Dhanasekaran, T., Govardhan, M., Nov. 2005. Computational analysis of performance and flow investigation on wells turbine for wave energy conversion. Renewable Energy 30 (14), 2129–2147.

Gato, L. M. C., de O. Falcao, A. F., 1988. Aerodynamics of the wells turbine. International Journal of Mechanical Sciences 30 (6), 383–395.

Gato, L. M. C., Webster, M., Jan. 2001. An experimental investigation into the effect of rotor blade sweep on the performance of the variable-pitch Wells turbine. Proceedings of the Institution of Mechanical Engineers, Part A: Journal of Power and Energy 215 (5), 611–622.

Govardhan, M., Dhanasekaran, T. S., 1998. Effect of Guide Vanes on the Performance of a Variable Chord Self-Rectifying Air Turbine. Journal of Thermal Science 7 (4).

Kim, T., Setoguchi, T., Kaneko, K., Raghunathan, S., Feb. 2002a. Numerical investigation on the effect of blade sweep on the performance of Wells turbine. Renewable Energy 25 (2), 235–248.

Kim, T., Setoguchi, T., Kinoue, Y., Kaneko, K., Oct. 2001. Effects of blade geometry on performance of wells turbine for wave power conversion. Journal of Thermal Science 10 (4), 293–300.

Kim, T. H., Setoguchi, T., Takao, M., Kaneko, K., Santhakumar, S., 2002b. Study of turbine with self-pitch-controlled blades for wave energy conversion. International Journal of Thermal Sciences 41 (1), 101–107.

Kinoue, Y., Setoguchi, T., Kim, T. H., Kaneko, K., Inoue, M., 2003. Mechanism of Hysteretic Characteristics of Wells Turbine for Wave Power Conversion. Journal of Fluids Engineering 125 (2), 302.

Puddu, P., Paderi, M., Manca, C., 2014. Aerodynamic Characterization of a Wells Turbine under Bi-directional Airflow. Energy Procedia 45, 278–287.

Raghunathan, S., 1995. The wells air turbine for wave energy conversion. Progress in Aerospace Sciences 31 (4), 335–386.

Setoguchi, T., Santhakumar, S., Maeda, H., Takao, M., Kaneko, K., 2001. A review of impulse turbines for wave energy conversion. Renewable Energy 23 (2), 261–292.

Setoguchi, T., Santhakumar, S., Takao, M., Kim, T. H., Kaneko, K., 2003. A modified Wells turbine for wave energy conversion. Renewable Energy 28 (1), 79–91.

Setoguchi, T., Takao, M., 2006. Current status of self rectifying air turbines for wave energy conversion. Energy Conversion and Management 47 (15-16), 2382–2396.

Setoguchi, T., Takao, M., Kaneko, K., 1998. Hysteresis on wells turbine characteristics in reciprocating flow. International Journal of Rotating Machinery 4 (1), 17–24.

Taylor, R. H., 1983. Alternative Energy Sources for the Centralised Generation of Electricity. Adam Hilger Ltd, Bristol.

Thakker, a., Abdulhadi, R., 2007. Effect of Blade Profile on the Performance of Wells Turbine under Unidirectional Sinusoidal and Real Sea Flow Conditions. International Journal of Rotating Machinery 2007, 1–9.

Thorpe, T., 2000. Wave Energy for the 21st century. Status and Prospects. Renewable Energy World, 115–121.

Wells, A., 1976. Fluid Driven Rotary Transducer - BR. Pat. 1595700.